

## 1

## Introduction of Bimetallic Nanostructures

Zhi-Ping Zhang and Ya-Wen Zhang

College of Chemistry and Molecular Engineering, Peking University, Beijing, China

### 1.1 Metallic Nanoparticles

Nanostructured particles are materials with at least one dimension at the nanoscale level (between 0.1 nm and 100 nm). Their scales are at the transition area between atomic clusters and bulk materials, and their optical, electrical, mechanical, magnetic, and catalytic properties are significantly different from those of bulk materials due to their quantum size effect, small size effect, surface effect, quantum tunneling effect, and dielectric confinement effect. There is no doubt that it is an exciting subject focusing on promising application of nanomaterials in various fields such as functional materials, sophisticated equipment, environmental remediation, and renewable energy processing.

In the elemental periodic table, more than two-thirds of the elements are metals. Metals are a class of glossy materials with good thermal and electrical conductivity, and are widely applied in architecture, electronic devices, information science, biomedical technology, and catalysis. For example, steel (iron) is often used for building; tungsten wire is applied in photoelectric instrument; ytterbium is applied in laser materials; and germanium is a valuable semiconductor material. Metal is fundamental to industry and life. In 1875, Pt/V<sub>2</sub>O<sub>5</sub> catalysts were applied in the large-scale production of sulfuric acid. Around 1913, Fe/Al<sub>2</sub>O<sub>3</sub>/K<sub>2</sub>O catalysts were used for ammonia synthesis, which was a significant reaction for the production of chemical fertilizer[1]. In the 1970s and 1980s, Pt, Pd, and Rh were developed for automobile emission control, including CO and HC oxidations and NO reduction[1].

In order to improve their material properties and enhance their atomic utilization efficiency, metallic materials were also manufactured in nanoscales. The preparation of metallic nanoparticles dates from 1850s. In 1857, Faraday synthesized his famous Au colloids through the reduction of Au(III) ions with phosphorous in water[2]. In 1941, Rampino and Nord prepared colloidal dispersion of Pd by reduction with hydrogen[3].

Attributed to the two main factors, unique surface effect and quantum size effect, metallic nanomaterials have exhibited different properties from the corresponding bulk

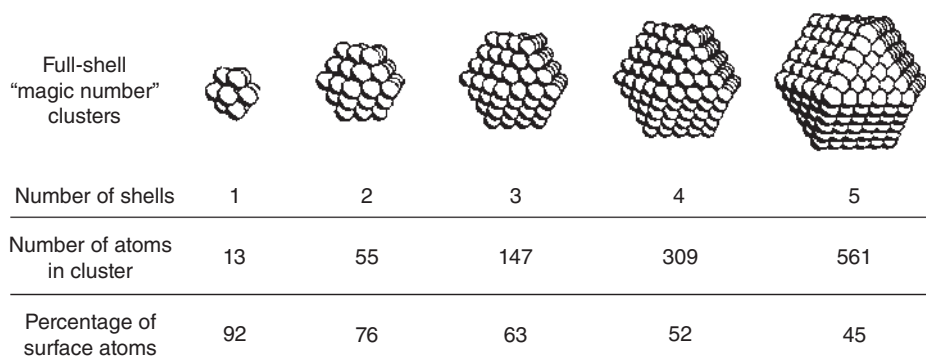


**Figure 1.1** The percentage of surface atoms with the change of the size of nanoparticles. Modified with permission from ref. [4], copyright 2009 Wiley-VCH.

materials and have attracted increasing attention due to their potential application in catalysis, plasmonic, sensing, magnetic recording and other fields. For example, Pt nanoparticles (NPs) are good catalysts for energy storage, Au NPs are candidates for photothermal therapy, Fe NPs are magnetic materials for spintronic devices. The first main factor, surface effect, results in the large surface-to-volume ratios of metallic nanoparticles (NPs). As shown in Figure 1.1, the percentage of surface atoms increases dramatically with the decreased size of nanoparticles[4]. So when the sizes of nanoparticles are decreasing, the distributions of low-coordinated or coordinatively unsaturated atoms, including corner, edge, kink and step sites, on the surface of small particles will be increasing. Unsaturated coordination environment gives rise to the strong trend of active surface atoms to capture other atoms or migrate, and leads to the change of electronic energy band, spin conformation of surface atoms. One example is the large difference of the melting points between bulk gold and 1.5 nm gold nanoparticles[5]. The former is 1064 °C, while the latter is reduced to ca. 500 °C. The lowered melting point of 1.5 nm gold nanoparticles is because the low-coordinated surface atoms dominate about 80% of the total atoms and are easily mobilized under thermal perturbation.

The second main factor, the quantum size effect, leads to the shifting electronic energy bands and the change of band gap between the highest occupied molecular orbital (HOMO) and the lowest unoccupied molecular orbital (LUMO). As shown in Figure 1.2, in one bulk metallic material, the effectively continuous energy band is the combination of an infinite number of very similar orbitals; and in individual atom, the energy band turns into discrete atomic orbitals; while the energy bands of a nanoparticle fall somewhere between continuous and discrete energy bands. Thus, it gives rise to the interesting phenomenon that the properties of nanoparticles are distinct from those of bulk materials, such as size-induced metal-insulator transition[6]. That is, most of bulk metals are conductors, but the electroconductivity of the corresponding metal NPs becomes weaker with the decreasing size, and these particles turn into insulators when their sizes are small enough. It depends on the magnitude between HOMO-LUMO gap (somewhere called the *Kubo gap*,  $\delta$ ) and thermal energy. Another famous example is the property change of gold (Au) with its size. Bulk Au material is a yellow metal with noble and nonmagnetic feature, but its corresponding 10 nm nanoparticles are red, its 2–3 nm nanoparticles are superior catalysts with magnetism, and its smaller clusters become insulators[6].

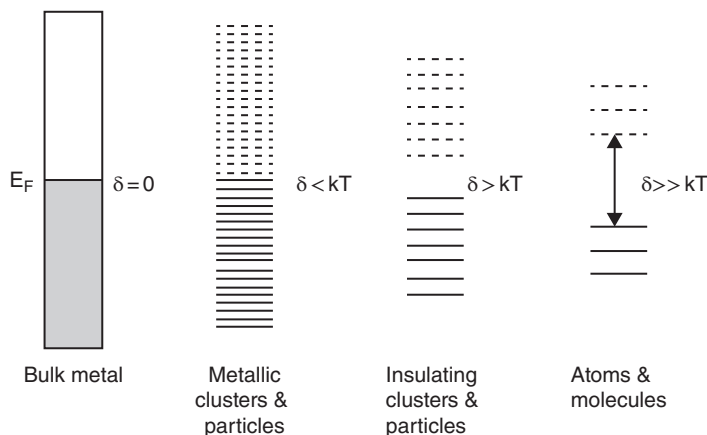


**Figure 1.2** The energy band and the density of states as the decreasing size of metallic materials.  $\delta$  is called the *Kubo gap*. Modified with permission from ref. [6], copyright 2006 Royal Society of Chemistry.

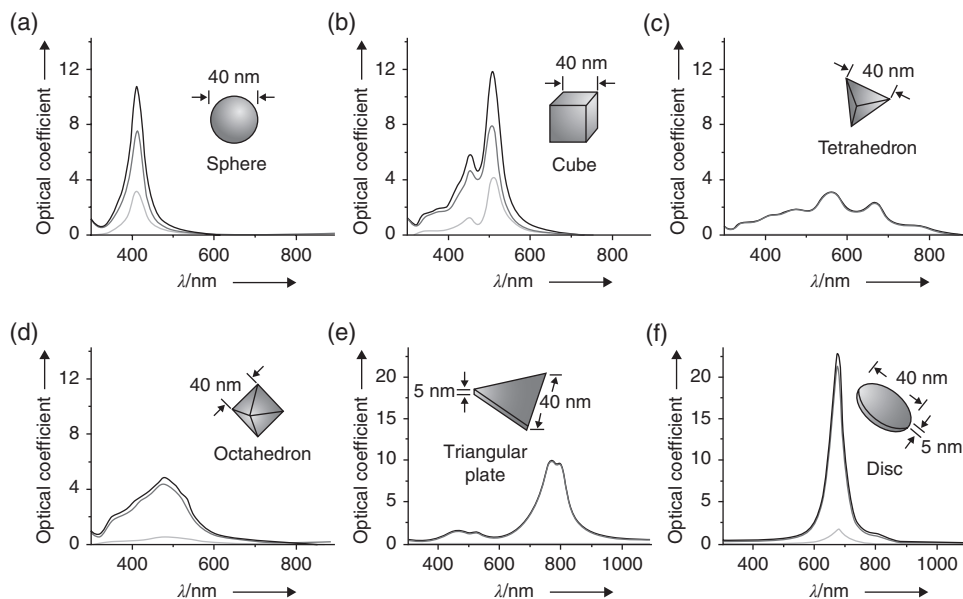


**Figure 1.3** Simulated UV-Visible spectra of Ag nanoparticles with different shapes but the same size of 40 nm. The top, middle and bottom curves in every panel represent extinction, absorption and scattering spectra, respectively. Reprinted with permission from ref. [4], copyright 2009 Wiley-VCH.

In addition to the size of metallic nanomaterials, their structure and shape also influence their intrinsic physical and chemical properties and their potential applications. One notable example is the different simulated UV-Visible spectra of Ag nanoparticles with different shapes but the same size of 40 nm, as illustrated in Figure 1.3. The number, intensity, and position of localized surface plasmon resonance (LSPR) peaks can be fine-tuned by shape control. They are dependent on the following three points [4]: (1) the number of LSPR peaks is determined by the number of ways in which the electron

density of a nanoparticle can be polarized; (2) the position of LSPR peaks can be tuned by altering corner sharpness and/or shape anisotropy; and (3) the intensity of LSPR peaks is affected by shape symmetry.

For Ag nanosphere, a strong dipole resonance at 410 nm and a weak quadrupole resonance at 370 nm are observed (Figure 1.3a). Recent calculations indicate that surface charges are mainly accumulated at sharp corners. This enhanced charge separation results in the reduced restoring force for electron oscillation and the red-shifted LSPR peak when all other parameters are comparable. Therefore, compared to the nanosphere, the most intense peaks of nanocube, nanotetrahedron, and nanooctahedron are red-shifted, and the largest red-shift exists on the nanotetrahedron due to its largest corner sharpness (Figure 1.3b–1.3d). Besides, the weakest intensity of LSPR peak also occurs on the nanotetrahedron due to its  $T_d$  symmetry. As shown in Figures 1.3e and 1.3f, compared with the triangular nanoplate, the intensity of LSPR peak of the nanodisc is much greater because the circular symmetry of the nanodisc can provide a greater effective dipole moment. The above example demonstrates that the properties of metallic nanoparticles are highly related to their shapes. Therefore, the precise control of their size, shape, distribution, and monodispersion is crucial for the property optimization of metallic nanoparticles. Within the past decades, many solution-phase methods have been developed to prepare the shape-controlled metallic nanoparticles through the manipulation of their nucleation and growth process.

## 1.2 Bimetallic Nanoparticles

Since the Bronze Age, humans have formed alloys simply by mixing or melting two metals. The hybrid bimetallic material could have more excellent properties (e.g., hardness, ductility, and malleability) than either one of the metals involved. For example, when alloying iron with copper and chromium, steel would exhibit enhanced mechanical properties in hardness, ductility and malleability, and improved resistance to corrosion.

In general, bulk alloyed materials must be melted at high temperatures, and most of the two kinds of metals in the bulk state are even immiscible. At the nanoscale level, however, the two metals may become miscible, and their melting point could decline substantially with the decrease of their size. This is because the formation of both enthalpy and Gibbs free energy of bimetallic materials decreases with particle size. Taking Cu–Ni as an example: although Cu–Ni has a positive formation enthalpy of the bulk immiscible system, Cu–Ni has a negative formation enthalpy when the particles are smaller than a critical size[7]. In this case, the alloying process first takes place in the dilute solute regions, then broadens to the dense solute regions, and finally forms the alloyed structure in the whole particle. It is apparent that bimetallic nanoparticles, composed of two distinct metal elements, are a new class of nanomaterials. On one hand, they exhibit different properties than their bulk bimetallic materials; on the other hand, they exhibit unique properties that differ from those of the corresponding pure monometallic counterparts and their physical mixings.

Modern interest in the synthesis and optical property of bimetallic nanoparticles dates from 1960s. In 1964, Morriss and Collins synthesized colloidal Au@Ag core-shell nanoparticles using 5.9 nm of Au nuclei, and compared their experimental optical

properties with the calculated results in different wavelength ranges[8]. In 1975, Papavassiliou discovered that the position of the absorption spectra of Au-Ag alloy solution depended on the composition of the alloy[9]. Commercial interest in bimetallic catalysts also dates from the 1960s due to their different activities toward hydrocarbon reforming from their parent metals[10]. The unexpected properties of bimetallic nanoparticles have inspired numerous further investigations on their syntheses, characterizations, properties, and applications.

Although bimetallic nanoparticles are more complicated than monometallic nanoparticles in many aspects, including synthesis control and structure characterization, they are superior in many ways. First, the incorporation of late transition elements, such as Fe, Co, and Ni, into the noble metallic nanoparticles can reduce the cost of materials, such as Pt–Ni alloy. Second, the electrical, physical, and chemical properties of bimetallic nanoparticles are not only associated with the two different metals but also can be modified easily by changing their composition, size, and shape. Furthermore, optimum components or an optimal structure of bimetallic nanoparticles can achieve a maximized atomic utilization rate and an excellent material property. The property modulation of bimetallic nanoparticles is mainly dependent on synergetic effects between two distinct elements, including electronic effect, lattice stress, bifunctional effect, and ensemble effect.

### 1.2.1 Electronic Effect

Electron transfer and charge redistribution occurs between two dissimilar atoms through d-state hybridization, and it gives rise to a change in density of state and d-band center of metal atoms. If the electronegativity of A is larger than that of B or B has a higher Fermi level, the electron will transfer from B to A, making the d-band center of A deeper and the d-band center of B shift up.

The adsorption energy of reaction species (reactant, intermediate, and product) on the metallic surface is related with the d-band center of the surface atoms, and further affects the catalytic activity. One example is Pt–M alloy nanocatalysts toward oxygen reduction reaction (ORR) (early-transition metals, M, include Y, Zr, Ti, Ni, and Co) investigated by Yoo et al.[11]. As shown in Figure 1.4, because early transition metals possess smaller electronegativity than Pt, the electrons flowed from M to Pt, which made the d-band center of Pt in the Pt–M NPs deeper and reduced the binding energy of the oxygen-containing species. Due to the volcano curve trend between the activity of ORR and the binding energy of the oxygen-containing species, Pt–M NPs exhibited the same volcano curve trend between the activity for ORR and the shifting d-band centers of Pt caused by the electronic perturbation of alloys. The d-band center of Pt and the binding energy of the oxygen-containing species in the Pt<sub>3</sub>Y NPs was the most appropriate, so that Pt<sub>3</sub>Y NPs exhibited the highest transition rate for adsorbed OH to water and further displayed the best activity toward ORR.

The electronic effect of multimetallic nanomaterials not only affects their catalytic property but also affects their optical property. Taking Au@Pd as an example, the LSPR peak of Au spheres was located at 524 nm. When the thickness of the Pd shell was 0.7 nm, the peak position was blue-shifted to 495 nm, attributed to the electron transfer from Pd to Au[12].

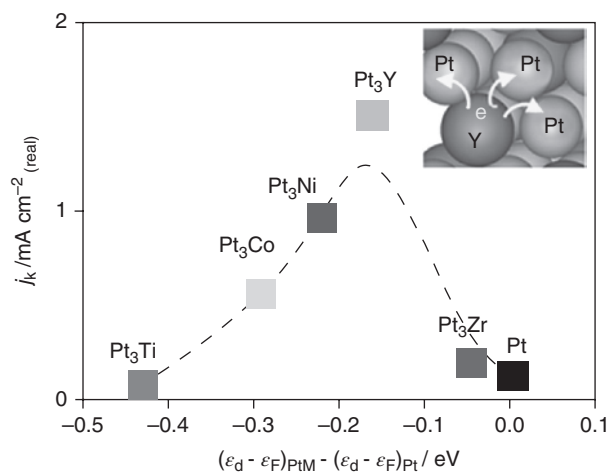


**Figure 1.4** Kinetic current density for ORR on Pt<sub>3</sub>M nanocatalysts and pure Pt nanocatalyst electrodes as a function of the d-band centers. Modified with permission from ref. [11], copyright 2012 American Chemical Society.

### 1.2.2 Lattice Stress

Lattice strain (compression or expansion) in core-shell or twin crystal caused by the different spatial arrangement of surface atoms results in a shift of d-band centers of metal or a change of d-band width; thus, it modulates the performance of bimetallic nanoparticles. A compressive strain causes a deeper d-band center of surface atom, and an expansive strain gives rise to a shallower d-band center of surface atom, as shown in Figure 1.5. As in the case of PtCu@Pt nanoparticles studied by Strasser and co-workers, the d-band centers of Pt in the Pt shell were modified by the compressive strain caused by the lattice mismatch between the Pt-rich shell and the PtCu core. Thus, it led to the weakened chemisorption of oxygenated species on the Pt shell, further giving rise to an enhanced catalytic reactivity toward ORR[13]. Predicted by density functional theory calculations, if the Pt–O binding energy ( $E_o$ ) on the surface of Pt-based nanoparticles is

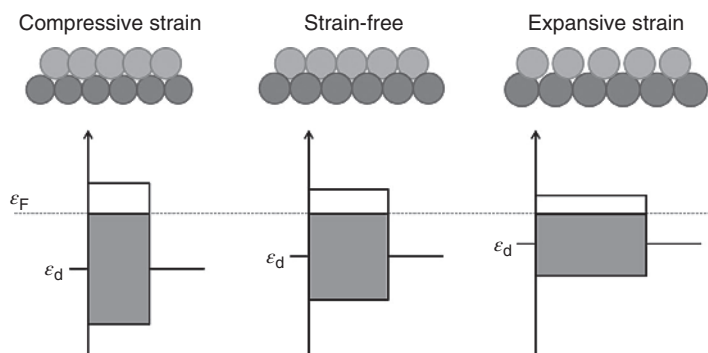


**Figure 1.5** The shift of d-band centers of metal attributed to the lattice strains.

0.2 eV higher than the value on the Pt (111) surface, the Pt-based nanoparticles will display the maximum ORR activity. So fct-FePt/Pt nanoparticles (fct, face-centered tetragonal) with the  $\Delta E_o$  of 0.23 eV exhibited higher activity than fcc-FePt/Pt nanoparticles (fcc, face-centered cubic) with the  $\Delta E_o$  of 0.26 eV toward ORR due to their smaller, overcompressed Pt strain[14].

### 1.2.3 Bifunctional Effect

The surfaces of bimetallic nanoparticles can offer multiple catalytic sites, which adsorb different reactant molecules or intermediates respectively. The adsorption of different reactant species on different sites can avoid the poison risk for active sites caused by competitive adsorption of different species on the same site. Besides, when each metallic component can catalyze different elementary reaction steps, the co-adsorption can be helpful for the transformation of reaction intermediates. For instance, for Pt monometallic electrocatalyst toward methanol oxidation reaction (MOR), CO is a poisoning species to Pt because of the strong bond energy of Pt–CO and the difficulty in the formation of the Pt–OH; while in the system of the Pt–Pd bimetallic catalysts, surface Pt sites catalyze the dehydrogenation of methanol to form Pt–CO, and surface Pd sites catalyze the dissociation of water to form Pd–OH, then Pt–CO reacts with Pd–OH to generate CO<sub>2</sub>, which regains Pt sites and enhances the reaction activity[15].

Furthermore, in the hybridization system of highly catalytic metals (e.g., Pt, Pd, or Rh) with plasmonic metals (e.g., Au, Ag, or Cu), the surfaces of bimetallic nanoparticles can offer multifunctional sites[16]. For example, Majima et al. demonstrated the plasmon-enhanced production of H<sub>2</sub> from water and methanol on Pt-tipped Au nanorods[17]. As illustrated in Figures 1.6a and 1.6b, upon irradiation with visible and near-IR light, the Au nanorod had the excellent capability to absorb light, then photoelectrons were transferred to the Pt-tips, and finally, the Pt-tips generated highly active catalytic activity to reduce H<sub>2</sub>O for the production of H<sub>2</sub>, while methanol was oxidized at the electron-deficient Au nanorod.

### 1.2.4 Ensemble Effect

In some cases of catalysis, specific groupings of surface atoms take on distinct mechanistic functionalities. For example, Magnussen et al. studied electrocatalysis in Pd/Au(111) electrodes. Pd monomer on Au(111) is the smallest ensemble for the adsorption and oxidation of CO, while H adsorption requires Pd dimers or larger ensembles[18]. Another example is the synthesis of vinyl acetate by coupling of ethylene and acetate on Pd–Au bimetallic catalysts prepared by deposition of Pd on Au surface investigated by Goodman et al.[19]. As shown in Figure 1.6c, ethylene and acetate were adsorbed on different Pd monomers, and the optimized distance is 3.3 Å, so the Pd–Au(100) with the distance between two neighboring Pd monomers of 4.08 Å exhibited higher activity than Pd–Au(111) surface with the distance of 4.99 Å (Figure 1.6d). The high activity of a Pd monomer for vinyl acetate formation is due to an ensemble effect—that is, Pd monomers isolated by Au could prevent the formation of byproducts.

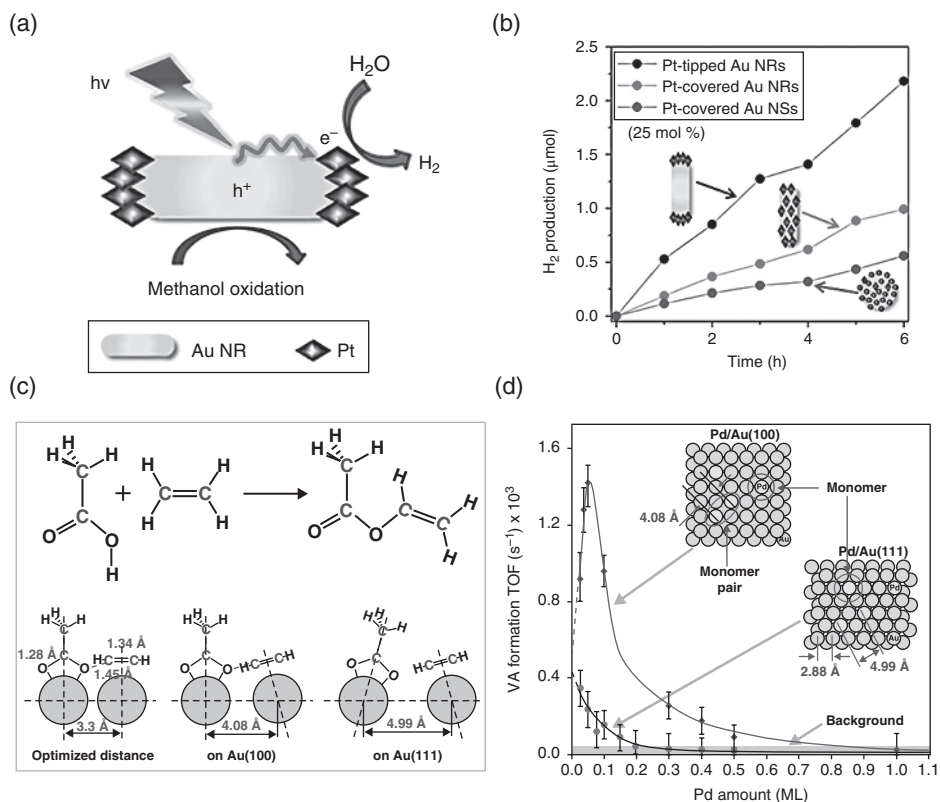


**Figure 1.6** (a) Reaction mechanism for H<sub>2</sub> production on Pt-tipped Au nanorods. (b) Time course of H<sub>2</sub> production on Pt-tipped Au nanoparticles under visible-light irradiation. Modified with permission from ref. [17], copyright 2014 American Chemical Society. (c) Schematic for vinyl acetate (VA) synthesis; (d) VA formation rates (TOFs) as a function of Pd coverage on Au(100) and Au(111). Modified with permission from ref. [19], copyright 2005 American Association for the Advancement of Science.

## 1.3 Bimetallic Nanostructures

The property and function application of bimetallic nanoparticles is heavily related with their structures. Bimetallic nanostructures are complicated and can be classified into three main types: alloyed structure (intermetallic or solid solution), core-shell, and heterostructure according to the mixing patterns of two different metals (A and B), as illustrated in Figure 1.7.

### 1.3.1 Alloyed Structure

Both of the two alloyed structures have homogeneous distribution of atom A and atom B, whether on the surface or inside the particle. The distributions of atom A and atom B in the intermetallic structure have long-range order (Figure 1.7a), while a solid-solution nanoparticle has a structure with a random distribution of atom A and atom B in the particle (Figure 1.7b). The atomic ordering in the intermetallic structure, such as Au<sub>3</sub>Cu, gives rise to a lattice structure distinct from the individual metals, and takes on

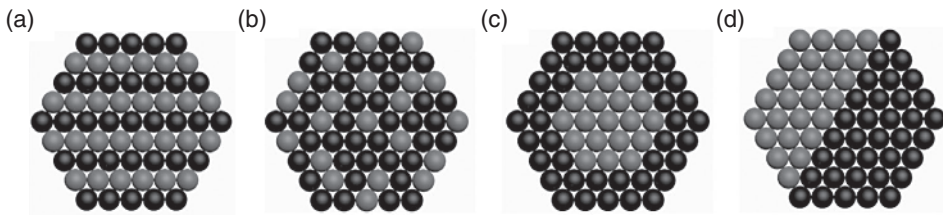


**Figure 1.7** Bimetallic nanostructures with different atomic arrangements: (a) intermetallic structure; (b) solid solution; (c) core–shell structure; (d) heterostructure.

a well-defined stoichiometry, rather than random mixing[16]. The solid-solution structure exhibits a single and new crystal phase, and the value of the lattice parameter is between that of A and that of B. For example, in PtCu<sub>3</sub> nanocage, its X-ray diffraction (XRD) pattern demonstrated the pure intermetallic PtCu<sub>3</sub> phase, and no obvious peaks of Pt or Cu were observed[20]. During the formation process of the alloyed structure, two metallic precursors are often reduced or decomposed simultaneously to form a single kind of crystal nucleus. Then two corresponding metallic atoms grow surrounding the nucleus. Another case is that one kind of metallic atoms (A) firstly forms a nanocrystal, then the other kind of metallic atoms (B) replaces part of A by galvanic replacement; or B diffuses into core A and A diffuses out to B shell, finally resulting in a homogeneous distribution of two distinct atoms.

### 1.3.2 Core–Shell

Core–shell nanoparticles have a boundary between the core and the shell, with one metal segregation (A or B) as the core and the other metal collection (B or A) as the shell, as illustrated in Figure 1.7c. One kind of metal precursor is reduced first, and it gives rise to the generation of an inner core. Then the other kind of metal precursor is decomposed into metallic atoms and grows on the surface of the core. Finally, a core–shell forms. The surface of the core–shell only exposes atom B or atom A. Generally speaking, the core–shell structure displays the phase of A and the phase of B simultaneously. The core–shell structure may be helpful for crystal phase structure of shell B to inherit that of core A, which is thermodynamically stable or even metastable for B. For example, the thermodynamic stable phase of Ru is hexagonal-close-packed (hcp), but in Pt@Ru (core–shell) nanotetrahedrons, shell Ru had the same phase (fcc) with core Pt due to the layered growth of Ru on the surface of fcc core Pt[21]. One reverse phenomenon may occur in the core-shell structure; that is, the phase transformation of core occurs simultaneously during the formation of core-shell. One example is the synthesis of fcc Au@Pt rhombic nanoplates through the epitaxial growth of Pt on hcp Au sheets [22]. Because the hcp phase was not a thermodynamic stable phase for core Au, the growth of shell Pt gave rise to the transformation of core A from the hcp phase to the fcc phase.

### 1.3.3 Heterostructure

The common types of heterostructures include dendritic structures, dimers, multipods, dumbbells, and Janus particles. In heterostructures, section A and section B share one or a few mixing interfaces, as shown in Figure 1.7d. The heterostructure displays the

phase of A and the phase of B simultaneously. In this kind of structure, atom A and atom B appear on different surfaces, respectively. If a secondary metal B is attached on one side of collection A by island growth instead of conformal overgrowth, heterostructure forms. For example, using the cubic Pt as seeds, Au was grown into a rod, adopting the anisotropic overgrowth on the Pt seed induced by large lattice mismatch (4.08% mismatch between Au and Pt). Finally, the Pt seed and the Au rod were both exposed in the heterostructure[23]. Liz-Marzán et al. demonstrated the synthesis of Ag–Au–Ag segmented nanorods through the deposition of Ag at both ends of Au nanorods using penta-twinned Au nanorods as seeds[24]. The length of bimetallic nanorods could be controllably grown to several micrometers and the thickness was increased only slightly, so their longitudinal resonant mode was greatly red-shifted. In another case, if individual nucleation and growth of A and B appear on a shared mixing interface and the deposition is nonepitaxial, heterostructure also forms.

### 1.3.4 Factors Affecting the Mixing Patterns

The mixing patterns of two different metals (A and B) not only are related with precise control over nucleation and growth processes but also depend on several factors[25]:

- 1) *Bond energy.* If the bond energy of A–B is stronger than that of A–A and that of B–B, one of the following two cases probably occurs. When the precursor of A and the precursor B are reduced or the atom A and the atom B deposit simultaneously, it tends to form the alloyed structure; and when the nanoparticles of A form preferentially, the atoms B will attach on the interface of A to form core–shell by layered growth. Otherwise, it tends to form a heterostructure.
- 2) *Surface energy.* The composition with lower surface energy tends to segregate on the surface of NPs. However, if the surface is decorated by surfactant or facet-specific capping agent, the surface will expose specific composition or specific facet.
- 3) *Atomic radius.* If the atomic radii of A and B are equal, it tends to form the alloyed structure or form core–shell by epitaxial growth. Otherwise, it tends to form a heterostructure by island growth.
- 4) *Charge transfer.* The electron transference between A and B favors the formation of A–B bond, which is helpful for mixing.
- 5) *Size of bimetallic nanoparticles.* Phase separation in bimetallic clusters is dependent on the size of nanoparticles, predicted by Monte Carlo simulation[26]. That is, the alloying effect in a nanoparticle of radius  $r$  is the result of the competition between the enthalpy of a demixing phase transformation and the interfacial energy required to create a new surface on demixing[27]. The enthalpy of demixing is proportional to  $r^3$  and the interfacial energy is proportional to  $r^2$ . So when the size of nanoparticles is small, the interfacial energy dominates, and it is less than enthalpy of demixing, the nanoparticles will stay as alloyed structure. Therefore, many of the two kinds of metals are immiscible in the bulk solid state but are miscible in the nanocluster state, such as Au and Pt.

## 1.4 Bimetallic Nanostructure-Dependent Performance

Different elemental composition ratios and various shapes of bimetallic materials have influences on their atomic arrangements, interactions between adjacent atoms, stacking patterns, and spatial atomic coordination environments. Since many physical and

chemical properties of bimetallic nanostructures are highly shape-dependent, surface-sensitive, and structure-sensitive, their promising functions can be optimized through the adjustment of various structure-dependent factors, including their composition, elemental distribution, size, geometric structure, and phase structure.

#### 1.4.1 Elemental Composition and Distribution-Property Correlation

The properties of bimetallic nanoparticles are intensively dependent on the intrinsic nature of the elemental compositions of the whole nanoparticles and the surface elemental distributions. For example, the catalytic activities of  $\text{Fe}_x\text{Pt}_{100-x}$  alloy nanoparticles with the average size of about 2.5 nm in the electro-oxidation of formic acid followed the order of  $\text{Fe}_{42}\text{Pt}_{58} > \text{Fe}_{54}\text{Pt}_{46} \approx \text{Fe}_{58}\text{Pt}_{42} > \text{Fe}_{15}\text{Pt}_{85} > \text{Fe}_{10}\text{Pt}_{90} > \text{Fe}_{63}\text{Pt}_{37}$ . The  $\text{Fe}_{42}\text{Pt}_{58}$  nanoparticles displayed the highest activity, the best stability, and the strongest tolerance to CO poisoning[28]. For alloyed structure of two plasmonic metals, the plasmon resonances of alloys can be interpolated between those of corresponding monometallic nanoparticle. An example is the tunable surface plasmon resonance (SPR) frequency of  $\text{Au}_x\text{Ag}_{100-x}$ . The SPR peak for  $\text{Au}_{0.82}\text{Ag}_{0.18}$ ,  $\text{Au}_{0.60}\text{Ag}_{0.40}$ ,  $\text{Au}_{0.52}\text{Ag}_{0.48}$ ,  $\text{Au}_{0.39}\text{Ag}_{0.61}$  nanoparticles of about 8 nm in sizes were 515 nm, 476 nm, 451 nm, 430 nm, respectively[29]. As illustrated in Figure 1.8, for the oxidation of toluene, the activity order of catalysts

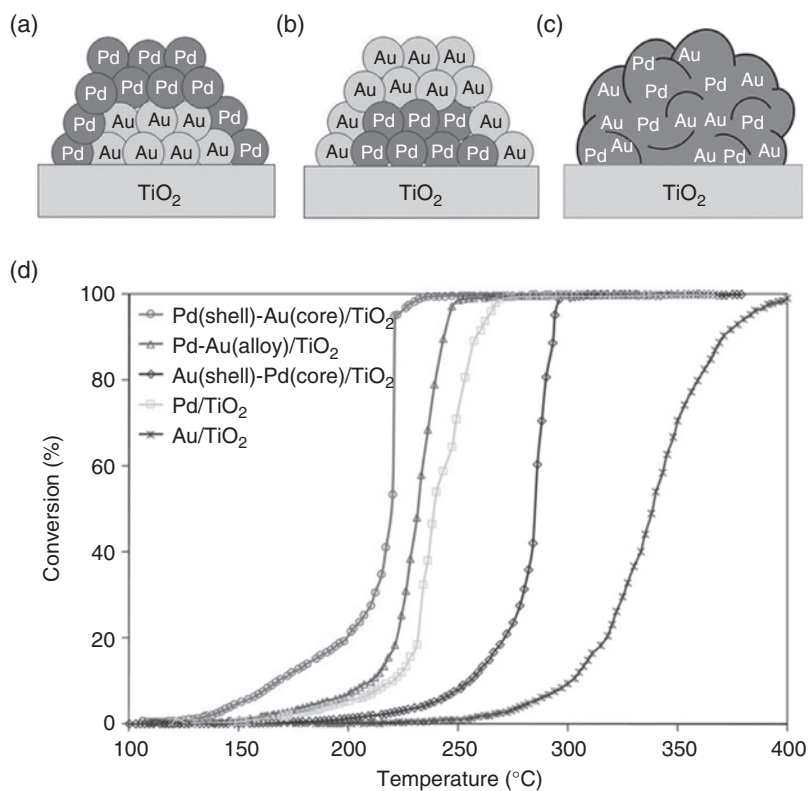


**Figure 1.8** Models proposed for: (a) Pd(shell)-Au(core)/ $\text{TiO}_2$ ; (b) Au(shell)-Pd(core)/ $\text{TiO}_2$ ; (c) Pd-Au(alloy)/ $\text{TiO}_2$ ; and (d) conversion of toluene on different catalysts. Modified with permission from ref. [30], copyright 2012 Elsevier.

followed Pd(shell)–Au(core)/TiO<sub>2</sub> > Pd–Au alloy/TiO<sub>2</sub> > Pd/TiO<sub>2</sub> > Au(shell)–Pd(core)/TiO<sub>2</sub> > Au/TiO<sub>2</sub>[30]. The reaction activity was dependent on the preferential adsorption of oxygen molecules on the surfaces of catalysts. Pd exhibited the higher affinity for oxygen than Au, so the catalytic activity of Pd/TiO<sub>2</sub> is higher than that of Au(shell)–Pd(core)/TiO<sub>2</sub> and Au/TiO<sub>2</sub>. The activity order of Pd(shell)–Au(core)/TiO<sub>2</sub> > Pd–Au alloy/TiO<sub>2</sub> > Pd/TiO<sub>2</sub> was due to the electronic promotion effect of Au for Pd.

#### 1.4.2 Size–Property Correlation

The properties of bimetallic nanoparticles are also dependent on their sizes. First, the miscibility and ordering of bimetallic structures are related with the size of nanoparticle. When the size is sufficiently small, the interface energy will overcome the enthalpy of demixing. Thus, it results in the formation of alloyed structure. For example, Au and Pt in the bulk state are immiscible, but form a random solid solution in nanoparticles with the radii less than 3 nm; 2–3 nm of CoPt NPs can transform from the disordered structure to the ordered structure at 773–923 K, while the transition point of the bulk CoPt is at 1023 K.

Besides, the size of bimetallic nanoparticle strongly affects its catalytic performance. With its decreasing size, bimetallic nanoparticle possesses an increased surface-to-volume ratio, a higher proportion of surface atoms, and a higher density of active sites such as atomic steps, edges, corners, and kinks. These sites exhibit abundant unsaturated coordination environments and dangling bonds, which make the adsorption of reactants easy and make the energy barriers lower. So the catalytic activity of small nanoparticles is often higher than that of large nanoparticles. However, sometimes the catalytic activity is not linearly dependent on the size. For example, as illustrated in Figure 1.9, Pd

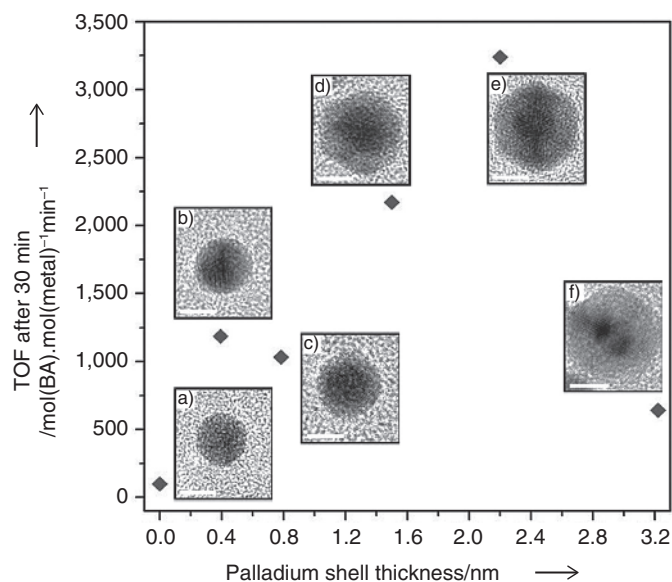


**Figure 1.9** Catalytic properties of icosahedral Au@Pd core@shell nanocrystals versus palladium shell thicknesses for the solvent-free oxidation of benzyl alcohol (BA). Modified with permission from ref. [31], copyright 2013 Wiley-VCH.

grew on the surface of Au core of 7.1 nm in size layer by layer, and this precise control of nucleation and growth rates enabled the synthesis of icosahedral Au@Pd with the tunable shell size ranging from 0.4 to 3.2 nm; when the Pd shell thickness was 2.2 nm, icosahedral Au@Pd had the maximum catalytic activity towards the oxidation of benzyl alcohol because of the optimized synergy between Au and Pd; while thinner or thicker shells resulted in lower activities[31].

Furthermore, the absorption wavelengths of plasmonic bimetallic nanoparticles display variation with their adjustable sizes. For example, when Ag shell on the Au nanorod thickened with the increased size of Au@Ag NP, Au@Ag NP exhibited a continuous blue-shift of extinction spectra and the color of corresponding solution changed from red to orange due to the alterant composition and aspect ratio of NP attributed to preferential side deposition rather than end deposition of Ag on the Au rod[32].

### 1.4.3 Geometric Structure-Property Correlation

The geometric structures of bimetallic nanoparticles can be classified into zero-dimensional (nanosphere, nanopolyhedron, nanoframe, convex, and concave), one-dimensional (nanowire, nanotube, nanorod), and two-dimensional structures (nanosheet, nanoplate, nanoribbon) according to the dimensionality of nanoparticles. The bimetallic nanoparticles with different morphologies expose different facets, exhibit different surface atomic arrangements, and possess distinct electronic distributions, which further lead to the tunable physical and chemical properties.

Zero-dimensional nanoparticles with fcc structure often possess low-index facets of  $\{111\}$ [1] and  $\{100\}$  as a result of the driving force of minimum total energy, and different polyhedrons exhibit different performances. For example, as shown in Figure 1.10a, Pt–Pd nanocubes with the exposed  $\{100\}$  facets displayed a higher activity than Pt–Pd nanotetrahedron with the exposed  $\{111\}$  facets toward MOR did[33].

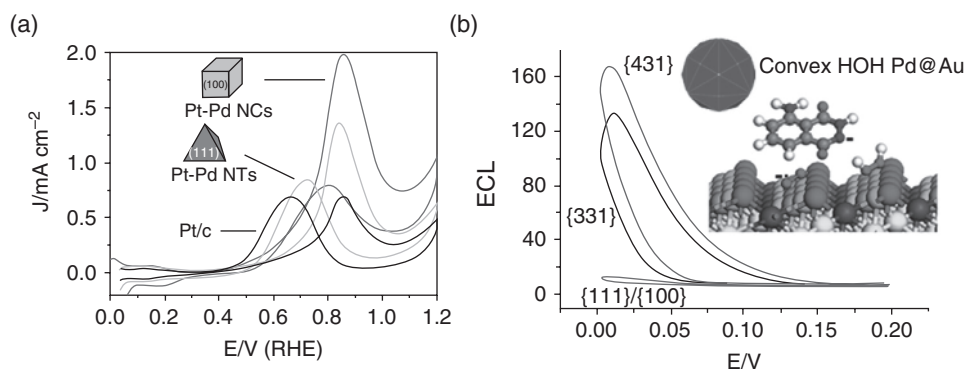


**Figure 1.10** (a) The activities of Pt-Pd nanocubes (NCs), Pt-Pd nanotetrahedrons (NTs) and Pt/C toward methanol oxidation reaction. Modified with permission from ref. [33], copyright 2011 American Chemical Society. (b) Electrochemiluminescence (ECL) potential curves of luminol/ $H_2O_2$  system on convex hexoctahedral (HOH), concave trisoctahedral, and truncated octahedral Pd@Au nanocrystal. Modified with permission from ref. [35], copyright 2014 American Chemical Society.

According to recent research, the coordination number of the surface atoms on a high-index facet is low due to the existence of abundant kinked, cornered, edged, and stepped atoms. These atoms are high-energy active sites. So sometimes synthesis methods could be optimized to obtain nanopolyhedrons with high-index facets. For example, hexoctahedral Au–Pd alloy NPs with  $\{hkl\}$  high-index facets were prepared through the assistance of  $\text{Cu}^{2+}$  ion by etching effect, and the NPs displayed excellent catalytic activity for formic acid oxidation and good tolerance to methanol[34]. Convex hexoctahedral Pd@Au NPs with  $\{431\}$  high-index facets were synthesized when combining fast-growth kinetics with capping effect, and they exhibited enhanced catalytic performances toward electrochemiluminescence compared to concave trisoctahedral Pd@Au NPs with  $\{331\}$  high-index facets and truncated octahedral Pd@Au NPs with  $\{111\}$  and  $\{100\}$  facets (Figure 1.10b) because of the abundant kink and step sites on  $\{431\}$  facets[35]. Highly branched concave Au/Pd NPs showed an improvement of surface-enhanced Raman spectra (SERS) due to their many intra- and interparticle gaps, tips, edges and hot spots[36].

Besides, porous nanoparticles and nanoframes often expose lots of highly unsaturated coordination sites (high-energy active sites), which lead to the enhanced catalytic activities[37]. For example,  $\text{Pt}_3\text{Ni}$  nanoframes achieved 36-fold increase in mass activities toward ORR when compared with Pt/C[38].

The dimensionality of nanomaterials plays an important role in their catalytic properties (activity, selectivity, and stability). The ultrathin features of one-dimensional or two-dimensional nanomaterials guarantee more accessible sites and unsaturated coordination sites, as well as accelerate reaction rates. For example, ultrathin Pt–Cu nanosheets displayed nine times higher activity than Pt/C for ethanol oxidation reaction[39]. Generally speaking, zero-dimensional NPs show lower stability with time due to their tendency to agglomerate and form larger particles in order to reduce surface area and surface energy; while one-dimensional NPs display higher stability due to the less agglomeration. Furthermore, the dimensionality change of nanomaterials can adjust their anisotropic property. Tunable aspect ratio of anisotropic plasmonic metallic particles gives rise to the change of surface plasmon resonance, including the resonance wavelengths and the resonance intensities. For example, Au/Ag nanorods show a much greater enhancement in local field and SERS activity than Au/Ag nanospheres do.

#### 1.4.4 Phase Structure-Property Correlation

$\text{A}_x\text{B}_y$  nanoparticles with diverse phase structures exhibit different properties due to their different bond distances of A–A, A–B, B–B, and different coordination environments. Different phase structures determine electronic energy level of metals and spatial distribution of constituent elements. For example, the FePt NPs with fcc structure (Figure 1.11a) were weakly superparamagnetic, while the FePt NPs with fct structure (Figure 1.11b) were ferromagnetic, and the latter displayed the better activity and durability than the former toward ORR (Figure 1.11c) because of their stable intermetallic stack of Fe and Pt[40]. The crystal phase of fcc Co@Pt nanocrystals could be transformed to homogeneous fct structure by annealing at 700 K. The former displayed zero coercivity, while the latter were ferromagnetic with a coercivity value of 5.3 kOe at room temperature[41].

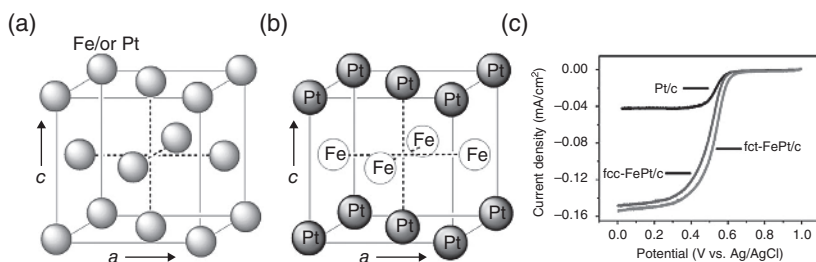


**Figure 1.11** Schematic illustration: (a) fcc-FePt; and (b) fct-FePt. ORR current densities from the commercial Pt/C, fcc-FePt/C, and fct-FePt/C catalysts. Modified with permission from ref. [40], copyright 2014 American Chemical Society.

## 1.5 Controlled Synthesis

The controlled synthesis of bimetallic nanostructures has attracted enormous interest because the property of bimetallic nanostructures is not only related with elemental nature, but also heavily dependent on the synthetic methods. Different methods affect the elemental distribution, size, geometric structure, and phase structure of bimetallic nanoparticles, further determining the performance of bimetallic nanoparticles. Precise control of the elemental distribution, size, geometric structure, and phase structure plays a valuable role in optimizing their functionality and application performance. Therefore, it is necessary to well understand the recent progress in the controlled synthesis of bimetallic nanostructures.

In the last few decades, several strategies have been achieved to prepare bimetallic nanostructures, including microwave, ultrasonic, sol-gel, microemulsion, and chemical precipitation. However, the controlled synthesis of bimetallic nanostructures still remain a challenge due to its complexity, such as its difficulty in ensuring synchronous nucleation and growth of different metals due to their distinct kinetic and thermodynamic properties.

The synthesis methods can be categorized into three kinds: solid-state method, gaseous-state method, and solution-state method[42]. The solid-state method needs long-time high-temperature heating and annealing, such as two kinds of bulk metals melting into alloys using metallurgy. The gaseous-state method requires complicated apparatus, such as mixed metallic vapors condense and form clusters or nanoparticles using chemical vapor deposition. The solution-state method is the most simple and powerful approach—for example, two metallic precursors being reduced and forming alloys simultaneously using thermal decomposition.

The solution-based approach can be classified into four types: continuous growth, crystallites coalescence, seeded-growth, and galvanic replacement[43], as shown in Figure 1.12. Several key factors, such as redox potentials of distinct metal precursors, surface tension and interface energy, surfactant and facet-specific capping agent, reducing agent, and experimental condition (concentration of reactants, mole ratio between precursors, temperature, time, atmosphere, pressure), should be controlled accurately in order to obtain monodisperse nanoparticles. By adjusting kinetic and thermodynamic factors, reduction rate or decomposition rate of metallic precursors can be optimized to trigger proper atomic packing styles and nucleation patterns. This further

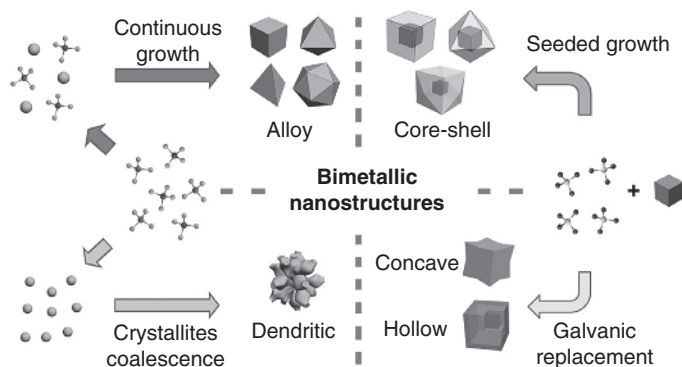


**Figure 1.12** Four solution-state-controlled synthesis routes of bimetallic nanostructure. Modified with permission from ref. [43], copyright 2012 Royal Society of Chemistry.

leads to expected growth process and finally determines the preparation output of well-defined bimetallic nanoparticles.

## 1.6 Outline of This Book

The main subject of this book is shape-controlled synthesis of bimetallic nanostructures for catalysis, plasmonics, and sensing application. The book is divided into three sections: the first one primarily introduces some basic chemical and physical knowledges of bimetallic structures, including fundamentals, computational models, and *in situ* characterization techniques; the second provides a brief summary of the recent development of synthetic methods, characterization methods, and properties of bimetallic structures from the perspective of morphology effect, including zero-dimensional nanomaterials, one-dimensional nanomaterials, and two-dimensional nanomaterials; and the last one illustrates applications of current interest derived from their properties.

A well-defined nanostructure provides a simple but clear physical model for the interpretation of structure-property relationship. The construction of calculation model and quantum computation for bimetallic nanostructures is helpful for the study of growth process and the mechanism of property. In Chapter 2 of Part One, we will address computational models of bimetallic nanostructure.

A variety of experimental characterization techniques, including electron microscopy, mass spectrometry, X-ray spectroscopy, and ultraviolet-visible spectroscopy, have been used to study structures and properties of bimetallic nanoparticles. Recently, the development of *in-situ* surface characterization makes it possible to track the growth process of bimetallic nanoparticles from atoms to nanostructures. Since the observation of the change on the surface of shape-controlled bimetallic nanoparticles in real time using *in situ* characterization is helpful to understand the nature of nanoparticles, we will focus on the *in situ* characterization techniques in Chapter 3 of Part One.

The chemical and physical properties of bimetallic nanoparticles are closely related to their structures, so shape control (including the atomic distributions on the surface and in the whole particle, size, geometric structure, and phase structure) of the bimetallic nanostructures is critical for the improvement and optimization of their tunable

physical and chemical properties. In Part Two, we will introduce the synthesis, characterization, and properties of shape-controlled bimetallic nanostructures, including zero-dimensional (Chapter 4 to Chapter 6), hierarchical and one-dimensional (Chapter 7 and Chapter 8), and two-dimensional (Chapter 9) structures.

Bimetallic nanostructures exhibit many interesting and unique properties, and their attractive properties make them applicable in different fields. In Part Three, we will describe some applications of shape-controlled bimetallic nanostructures, including electrocatalysis in Chapter 10, heterogeneous catalysis in Chapter 11, plasmonics in Chapter 12, and sensing in Chapter 13.

The book is addressed to a wide circle of academic researchers in nanoscience, nanotechnology, and nanomaterial, and to those working in the areas of industry including nanotechnology, catalysis, and optoelectronics. A systematic summary of controlled synthesis, characterization, properties, and applications of well-defined bimetallic nanostructures in this book is helpful for establishing a comprehensive grasp of fundamental knowledge and recent development of bimetallic nanoparticles.

## 1.7 References

- 1 Bartholomew, C. H., and Farrauto, R. J. (2006). Fundamentals of Industrial Catalytic Processes. *Fundamentals of Industrial Catalytic Processes*, 2nd ed. Hoboken, NJ: John Wiley & Sons, Inc.
- 2 Faraday, M. (1857). *Philos. Trans. R. Soc. London*, 147.
- 3 Rampio, L. D., and Nord, F. F. (1941). Applicability of palladium synthetic high polymer catalysts. *Journal of the American Chemical Society*, 63 (12), 3268–3268.
- 4 Xia, Y., Xiong, Y., Lim, B. and Skrabalak, S. E. (2009). Shape-controlled synthesis of metal nanocrystals: simple chemistry meets complex physics? *Angewandte Chemie-International Edition*, 48 (1), pp. 60–103.
- 5 Corain, B., Schmid, G. and Toshima, N. (2008). metal nanoclusters in catalysis and materials science: the issue of size control. Amsterdam: Elsevier.
- 6 Roduner, E. (2006). Size matters: why nanomaterials are different. *Chemical Society Reviews*, 35 (7), 583–592.
- 7 Qi, W. (2016). Nanoscopic thermodynamics, *Accounts of Chemical Research*, 49 (9), 1587–1595.
- 8 Morriss, R. H., and Collins, L. F. (1964). Optical properties of multilayer colloids. *Journal of Chemical Physics*, 41 (11), 3357–3363.
- 9 Papavassiliou, G. C. (1976). Surface-plasmons in small Au–Ag alloy particles. *Journal of Physics F-Metal Physics*, 6 (4), L103–L105.
- 10 Sinfelt, J. H. (1977). Catalysis by alloys and bimetallic clusters, *Accounts of Chemical Research*, 10 (1), 15–20.
- 11 Hwang, S. J., Kim, S. K., Lee, J. G., Lee, S. C., Jang, J. H., Kim, P., Lim, T. H., Sung, Y. E. and Yoo, S. J. (2012). Role of electronic perturbation in stability and activity of Pt-based alloy nanocatalysts for oxygen reduction, *Journal of the American Chemical Society*, 134 (48), 19508–19511.
- 12 Zhang, L., Xie, Z. X., and Gong, J. L. (2016). Shape-controlled synthesis of Au-Pd bimetallic nanocrystals for catalytic applications, *Chemical Society Reviews*, 45 (14), 3916–3934.

- 13 Strasser, P., Koh, S., Anniyev, T., Greeley, J., More, K., Yu, C., Liu, Z., Kaya, S., Nordlund, D., Ogasawara, H., Toney, M. F. and Nilsson, A. (2010). Lattice-strain control of the activity in dealloyed core-shell fuel cell catalysts, *Nature Chemistry*, 2 (6), 454–460.
- 14 Zhang, S., Zhang, X., Jiang, G. M., Zhu, H. Y., Guo, S. J., Su, D., Lu, G. and Sun, S. H. (2014). Tuning nanoparticle structure and surface strain for catalysis optimization, *Journal of the American Chemical Society*, 136 (21), 7734–7739.
- 15 Liu, Y., Chi, M., Mazumder, V., More, K. L., Soled, S., Henao, J. D. and Sun, S. (2011). Composition-controlled synthesis of bimetallic PdPt nanoparticles and their electro-oxidation of methanol, *Chemistry of Materials*, 23 (18), 4199–4203.
- 16 Gilroy, K. D., Ruditskiy, A., Peng, H. C., Qin, D. and Xia, Y. (2016). Bimetallic nanocrystals: syntheses, properties, and applications, *Chemical Reviews*, 116 (18), 10414–10472.
- 17 Zheng, Z. K., Tachikawa, T. and Majima, T. (2014). Single-particle study of Pt-modified Au nanorods for plasmon-enhanced hydrogen generation in visible to near-infrared region, *Journal of the American Chemical Society*, 136 (19), 6870–6873.
- 18 Maroun, F., Ozanam, F., Magnussen, O. M. and Behm, R. J. (2001). The role of atomic ensembles in the reactivity of bimetallic electrocatalysts, *Science*, 293 (5536), 1811–1814.
- 19 Chen, M. S., Kumar, D., Yi, C. W. and Goodman, D. W. (2005). The promotional effect of gold in catalysis by palladium-gold, *Science*, 310 (5746), 291–293.
- 20 Xia, B. Y., Wu, H. B., Wang, X. and Lou, X. W. (2012). One-pot synthesis of cubic PtCu<sub>3</sub> nanocages with enhanced electrocatalytic activity for the methanol oxidation reaction, *Journal of the American Chemical Society*, 134 (34), 13934–13937.
- 21 Gu, J., Guo, Y., Jiang, Y. Y., Zhu, W., Xu, Y. S., Zhao, Z. Q., Liu, J. X., Li, W. X., Jin, C. H., Yan, C. H. and Zhang, Y. W. (2015). Robust phase control through hetero-seeded epitaxial growth for face-centered cubic Pt@Ru nanotetrahedrons with superior hydrogen electro-oxidation activity, *Journal of Physical Chemistry C*, 119 (31), 17697–17706.
- 22 Fan, Z., Zhu, Y., Huang, X., Han, Y., Wang, Q., Liu, Q., Huang, Y., Gan, C. L. and Zhang, H. (2015). Synthesis of ultrathin face-centered-cubic Au@Pt and Au@Pd core-shell nanoplates from hexagonal-close-packed Au square sheets, *Angewandte Chemie-International Edition*, 54 (19), 5672–5676.
- 23 Habas, S. E., Lee, H., Radmilovic, V., Somorjai, G. A. and Yang, P. (2007). Shaping binary metal nanocrystals through epitaxial seeded growth, *Nature Materials*, 6 (9), 692–697.
- 24 Mayer, M., Scarabelli, L., March, K., Altantzis, T., Tebbe, M., Kociak, M., Bals, S., de Abajo, F. J. G., Fery, A. and Liz-Marzan, L. M. (2015). Controlled living nanowire growth: precise control over the morphology and optical properties of AgAuAg bimetallic nanowires, *Nano Letters*, 15 (8), 5427–5437.
- 25 Ferrando, R., Jellinek, J. and Johnston, R. L. (2008). Nanoalloys: from theory to applications of alloy clusters and nanoparticles, *Chemical Reviews*, 108 (3), 845–910.
- 26 Christensen, A., Stoltze, P. and Norskov, J. K. (1995). Size dependence of phase-separation in small bimetallic clusters, *Journal of Physics-Condensed Matter*, 7 (6), 1047–1057.
- 27 Cortie, M. B. and McDonagh, A. M. (2011). Synthesis and optical properties of hybrid and alloy plasmonic nanoparticles, *Chemical Reviews*, 111 (6), 3713–3735.

- 28 Chen, W., Kim, J. M., Sun, S. H. and Chen, S. W. (2007). Composition effects of fept alloy nanoparticles on the electro-oxidation of formic acid, *Langmuir*, 23 (22), 11303–11310.
- 29 Wang, C., Yin, H., Chan, R., Peng, S., Dai, S. and Sun, S. (2009). One-pot synthesis of oleylamine coated AuAg alloy NPs and their catalysis for CO oxidation, *Chemistry of Materials*, 21 (3), 433–435.
- 30 Hosseini, M., Barakat, T., Cousin, R., Aboukais, A., Su, B. L., De Weireld, G. and Siffert, S. (2012). Catalytic performance of core-shell and alloy Pd–Au nanoparticles for total oxidation of VOC: The Effect of Metal Deposition, *Applied Catalysis B-Environmental*, 111 pp. 218–224.
- 31 Henning, A. M., Watt, J., Miedziak, P. J., Cheong, S., Santonastaso, M., Song, M., Takeda, Y., Kirkland, A. I., Taylor, S. H. and Tilley, R. D. (2013). Gold-palladium core-shell nanocrystals with size and shape control optimized for catalytic performance, *Angewandte Chemie-International Edition*, 52 (5), 1477–1480.
- 32 Zhang, C., Yin, A. X., Jiang, R., Rong, J., Dong, L., Zhao, T., Sun, L. D., Wang, J., Chen, X. and Yan, C. H. (2013). Time-temperature indicator for perishable products based on kinetically programmable Ag overgrowth on Au nanorods, *ACS Nano*, 7 (5), 4561–4568.
- 33 Yin, A. X., Min, X. Q., Zhang, Y. W. and Yan, C. H. (2011). Shape-selective synthesis and facet-dependent enhanced electrocatalytic activity and durability of monodisperse Sub-10 nm Pt-Pd tetrahedrons and cubes, *Journal of the American Chemical Society*, 133 (11), 3816–3819.
- 34 Zhang, L., Zhang, J., Kuang, Q., Xie, S., Jiang, Z., Xie, Z. and Zheng, L. (2011). Cu<sup>2+</sup>-assisted synthesis of hexoctahedral Au-Pd alloy nanocrystals with high-index facets, *Journal of the American Chemical Society*, 133 (43), 17114–17117.
- 35 Zhang, L., Niu, W., Gao, W., Qi, L., Lai, J., Zhao, J. and Xu, G. (2014). Synthesis of convex hexoctahedral palladium@gold core-shell nanocrystals with {431} high-index facets with remarkable electrochemiluminescence activities, *Acs Nano*, 8 (6), 5953–5958.
- 36 Zhang, L. F., Zhong, S. L. and Xu, A. W. (2013). Highly branched concave Au/Pd bimetallic nanocrystals with superior electrocatalytic activity and highly efficient SERS enhancement, *Angewandte Chemie-International Edition*, 52 (2), 645–649.
- 37 Zhang, Z. P., Zhu, W., Yan, C. H. and Zhang, Y. W. (2015). Selective synthesis of rhodium-based nanoframe catalysts by chemical etching of 3d metals, *Chemical Communications*, 51 (19), 3997–4000.
- 38 Chen, C., Kang, Y., Huo, Z., Zhu, Z., Huang, W., Xin, H. L., Snyder, J. D., Li, D., Herron, J. A., Mavrikakis, M., Chi, M., More, K. L., Li, Y., Markovic, N. M., Somorjai, G. A., Yang, P. and Stamenkovic, V. R. (2014). Highly crystalline multimetallic nanoframes with three-dimensional electrocatalytic surfaces, *Science*, 343 (6177), 1339–1343.
- 39 Saleem, F., Zhang, Z., Xu, B., Xu, X., He, P. and Wang, X. (2013). Ultrathin Pt-Cu nanosheets and nanocones, *Journal of the American Chemical Society*, 135 (49), 18304–18307.
- 40 Kim, J., Lee, Y. and Sun, S. H. (2010). Structurally ordered FePt nanoparticles and their enhanced catalysis for oxygen reduction reaction, *Journal of the American Chemical Society*, 132 (14), 4996–4997.

- 41 Park, J. I., Kim, M. G., Jun, Y. W., Lee, J. S., Lee, W. R. and Cheon, J. (2004). Characterization of superparamagnetic “core-shell” nanoparticles and monitoring their anisotropic phase transition to ferromagnetic “solid solution” nanoalloyse, *Journal of the American Chemical Society*, 126 (29), 9072–9078.
- 42 Wang, D. and Li, Y. (2011). Bimetallic nanocrystals: liquid-phase synthesis and catalytic applications, *Advanced Materials*, 23 (9), 1044–1060.
- 43 Gu, J., Zhang, Y. W. and Tao, F. (2012). Shape control of bimetallic nanocatalysts through well-designed colloidal chemistry approaches, *Chemical Society Reviews*, 41 (24), 8050–8065.